https://dx.doi.org/10.1016/j.applthermaleng.2021.117176

An innovative thermal management method for cooling loop of electric driving system of electric vehicle

Dongjun Li[1], Caizhi Zhang[1*], Ruijia Fan[1], Lei Xu [2], Yi Wang [2], Wenjun Guo [2], Jinrui Chen [4], Meng Ni [5*]

[1] School of Automotive Engineering; The State Key Laboratory of Mechanical Transmissions; Chongqing Automotive Collaborative Innovation Center, Chongqing University, Chongqing, China, 400044

[2] China Automotive Engineering Research Institute Co., Ltd., China, 401120

[3] Propulsion Research Institute of Chongqing Changan New Energy Vehicle Technology Co., Ltd, Chongqing, China, 400000

[4] Department of Building and Real Estate, Building Energy Research Group, The Hong Kong Polytechnic University, Hung Hom, Kowloon, Hong Kong, China

** Corresponding Authors:*

Caizhi Zhang (czzhang@cqu.edu.cn) and Meng Ni (meng.ni@polyu.edu.hk)

Abstract: This paper proposed an innovative thermal management framework and its control strategies for cooling loop of electric drive system of electric vehicle to achieve a more refined thermal management. The proposed innovative framework (IF) models of cooling loop of electric drive were developed in KULI based on the heating principle of each key component and heat transfer theory. The cooling loop model of electric drive system was composed of triad (High Voltage Junction Box, On-Board Charger and DC/DC), motor controller, motor, radiator, cooling fan and pump. The rule-based control strategies were established in MATLAB/Simulink based on the output coolant temperature of triad, motor controller and motor. It is as a controller running with of VTMS models in KULI. To verify performance, the conventional framework (CF) model derived from an electric vehicle was also implemented. Then, the cooling performance of cooling loop of electric drive and the energy consumption of the two frameworks were compared through co-simulation under steady-stage and transient condition of high temperature. The results showed that new method has a better performance in temperature control of key components, exit temperature of motor reduced at least 5.03 ºC under 3 steady-stage simulation condition, and efficiency of cooling pump, which is useful to thermal management system design to decrease energy consumption.

Keywords: cooling loop of electric drive, thermal management, control strategies, energy consumption

1. Introduction

Increasingly stringent legislations of emission have brought great challenges for the transportation. Electric vehicle has captured wide attention due to the merits of zero emission, high efficiency as well as quiet operation [1-3]. Compared to conventional vehicles, power source is substituted by electric motors converting the electrical power provided by Li-batteries or fuel cell into mechanical energy [4-6]. The working performance of electrical equipment (e.g., Li-battery, motor, motor controller, DC/DC) is sensitive to operating thermal conditions. For example, in order to achieve the optimum performance and long service life, the operating temperature range of Li-battery must be maintained at 15~35ºC [2, 7]. In addition, the optimum operating temperature of various electrical devices (e.g., motor operating temperature range is 10-70 ºC , DC/DC operating temperature range is 10-55ºC) deviate largely [8-10]. Only under the appropriate operating temperature, electronic components can have high efficiency and durability. Therefore, cooling loop of electric drive needs to be deeply investigated.

Vehicle Thermal Management System (VTMS) has attracted high attention in recent years, because it has the ability to redistribute and reroute thermal energy around the vehicle and to enables quicker component conditioning to optimal operating conditions [10, 11]. To alleviate energy loss during electric vehicle operation process, several significant thermal management technics, control strategies and thermal management schemes of VTMS are prompted in recent years, such as waste heat recovery technic, heat pump technic and new materials [12-15]. Waste heat recovery technology is one of the important technologies of VTMS to improve the performance of the thermal management system of new energy vehicles [16]. It rationally uses the heat from the high temperature heat source on the new energy vehicles to heat the vehicle battery pack, resulting in improving the driving range of new energy vehicles [17-19]. Moreover, heat pump (HP) becomes a popular way to transfer thermal energy throughout vehicle systems. The heat pump system with the utilization of refrigerant latent heat could achieve higher energy efficiency and reduce electricity consumption [20-22]. With improvement of HP performance, modifications have been proposed including vapor injection, refrigerant substitutes and mixtures, combined defrost methods, integrated desiccant, and sorption [1, 11, 23-26]. In addition, more and more control algorithms and control strategies are applied to VTMS, such as robust predictive strategy [27], nonlinear model predictive control [28], fuzzy control and self-adaptive control etc. [8]. On careful inspection, the aforementioned studies are aimed to increase the utilization rate of energy by reusing waste heat or more precise control, and new thermal management technologies. And current research on thermal management systems is mostly focused on battery packs or air-conditioning systems. However, as the core power source of electric vehicle, it is also very important to realize the refined thermal

management of the electric drive circuit. Not only the waste heat generated by the electric drive system can be used as the heat source for waste heat recovery, but also the different working temperature range of electronic components can be used to realize more refined thermal management of pump and fan through VTMS.

The water-cooling pattern is adopted in cooling loop of electric drive in EVs, which is more than 50 times of air-cooling volume [29, 30]. At present, the research on thermal management of electric drive system is mostly independent component research, such as the cooling performance of motor, etc., rarely discussed the thermal management performance of electric drive system from the perspective of vehicle loop [31-33]. On the other hand, the cooling loop of the electric drive adopts the one-way circulation cooling mode, and the control research of the related thermal management system also focuses on the optimal control of the water pump [8, 10]. In addition, in the formulation of the VTMS control strategy of the electric drive circuit, when the operating temperature of an electric device in the circuit reaches its threshold temperature, the speed of the pump or fan is increased to improve the heat dissipation. Those are reasonable and effective methods, but it does not take full advantage of the differences in the working temperature of components of cooling loop of electric drive. However, if the coolant flow ratio can be distributed according to cooling demand of electric devices, operating temperature of the electric devices can be guaranteed within the threshold without changing the speed of the pump and fan, which may reduce the energy consumption of pump and fan.

Therefore, this paper proposed an innovative thermal management method for cooling loop of automotive electric drive through changing the framework and control strategy of cooling loop of electric drive of VTMS. Compared with the conventional framework (CF) of cooling loop of electric drive, the innovative thermal management method includes an electrically controlled proportional valve and two three-way valves, as well as a control strategy for the electrically controlled proportional valve to realize fine thermal management of cooling loop of electric drive. Cooling loop of electric drive models, based on a commercial electric vehicle, are established KULI and MATLAB/Simulink. The co-simulation results show that the innovative thermal management control method realized the refined thermal management of cooling loop of electric drive under several drive cycles, especially energy consumption and temperature control.

2. Electric drive thermal management system

2.1 System description

Figure 1 shows a vehicle thermal management system (VTMS) of an EV, which include four cooling or heating loops. In this VTMS, cooling pump, cooling fan and radiator are components used to cool the loop of electric drive. The loop of lithium battery is cooled by a double channel chiller, and heated by a

heater core body and a 50W pump. Besides, the refrigerant in air condition loop is 1,1,1,2-tetrafluoroethane (R-134a), which generally used in automotive applications. And water/glycol (50%/50%) mixture is adopted as coolant in other loops due to the mixture has a lower viscosity and higher thermal conductivity than most oils, resulting in higher heat transfer coefficients more than 50 times higher than air [30, 34].

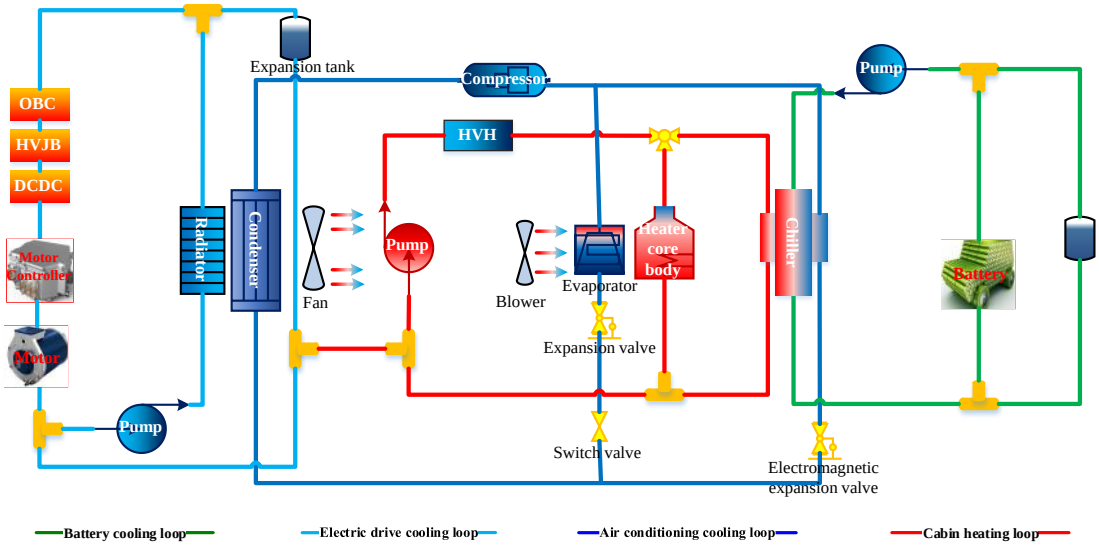

Figure 1. Scheme of vehicle thermal management system

2.2 Conventional framework of cooling loop of electric drive

In view of the pith of this paper is cooling loop of electric drive, Figure 2 (a) shows the CF of cooling loop of electric drive of the VTMS, which is composed of on-board charger (OBC), high voltage junction box (HVJB), DC/DC, motor controller (MCU), motor, a 37W cooling pump, a 320W cooling fan and a radiator. Due to different suitable temperature of MCU, motor and other electric components, the coolant of cooling loop of electric drive in the conventional thermal management framework adopted a unidirectional flow from low to high. Therefore, the volume flow rate in cooling loop of electric drive can be considered to be equal everywhere.

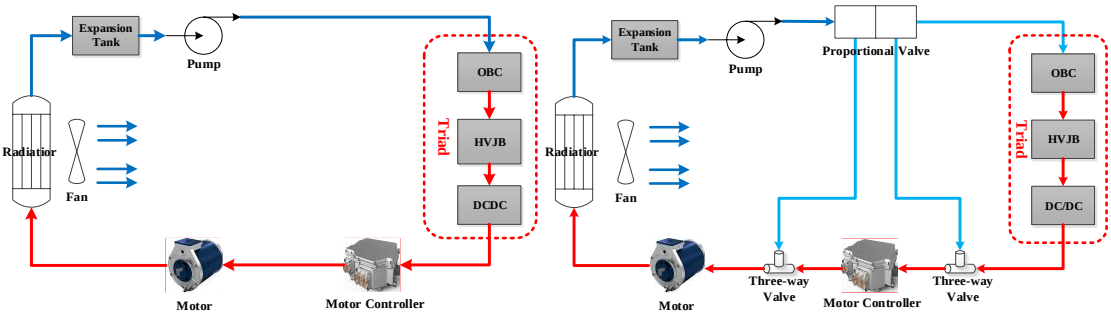

Figure 2. Framework of electric drive cooling loop of electric drive (a) Innovative framework (b) Conventional framework

In Figure 2 (a), the triad (consisted of OBC, HVJB and DC/DC), motor controller and motor dissipate

heat when the vehicle is in motion. In this paper, the optimal operating temperature range of triad, MCU and motor is -20-65ºC, -40-65 ºC and -40-70 ºC respectively [8, 35]. Heat absorbed from the electronic components is released by heat exchange between the air and the high temperature coolant through the radiator. Fan and water pump are used as cooling power devices to enhance the cooling effect of the drive circuit by increasing the flow of air and coolant through the radiator. The expansion tank was used to compensate the thermal expansion of the fluid generated by the temperature rise, and at the same time remove the air from the coolant.

2.3 The proposed framework of cooling loop of electric drive

Figure 2 (b) shows an innovative framework (IF) of cooling loop of electric drive by adding proportional valve, three-way valves and pipes in the traditional VTMS. In this IF, the coolant flowing through the proportional valve can be divided into three 3 parts, one-part through the Triad (OBC, HJBX and DC/DC), MCU and motor, one-part through the MCU and motor only, and the last part through the motor only. The function of three-way value is to converge the coolant. This framework of branch and converging allows more precise control of cooling power of each electric component. In particular, heat transfer theory shows that changing the cooling flow rate may affect the heat loss in the heat dissipation process. Therefore, the fine thermal management of electric components may achieve by the control of each branch coolant flow by a proportional valve.

3. System modelling

3.1 Heat generation model motor, MCU and triad

In this paper, an electric vehicle with the specification shown in Table 1 is investigated. In Vehicle dynamics [3, 36], the equations (1)-(6) show the relationship between the driving force and the driving resistance including rolling resistance F_f, grade resistance F_i, air friction F_w and acceleration resistance F_j. Besides, the driving force can be calculated by the motor torque T_m, the driving force F_t generated by the electric motor converting the electrical power provided by lithium battery into mechanical energy for operating.

$$F_t = F_f + F_w + F_i + F_j \quad (1)$$

$$F_t = \frac{T_m i_0 \eta_T}{r} \quad (2)$$

$$F_f = mgf\cos\alpha \quad (3)$$

$$F_w = \frac{C_D A_v u_a^2}{21.15} \quad (4)$$

$$F_i = mg\sin\alpha \quad (5)$$

$$F_j = \delta m \frac{du_a}{dt} \tag{6}$$

where i_0 is the vehicle transmission ratio; η_T is the transmission efficiency; r is the tire radius; m is the vehicle mass; g is the acceleration of gravity; f is the rolling resistance coefficient; α is the climbing angle; C_D is the air drag coefficient; A_v is the front area; u_a is the vehicle velocity; δ is the correction coefficient of rotating mass. The motor speed and electric power can be calculated as equation (7) and (8).

$$n = \frac{60 i u_a}{2\pi r} \tag{7}$$

$$P_m = \frac{T_m \times n}{9550 \eta_m} \tag{8}$$

where η_m is the motor efficiency obtained from the bench text of motor.

Table 1. Specification of the battery vehicle

Parameter	Symbol	Unit	Value
Weight	m	Kg	1812.06
Transmission ratio	i_0	-	9.11
Transmission efficiency	η_T	-	95%
Tire radius	r	m	0.355
Acceleration of gravity	g	-	9.8
Rolling resistance coefficient	f	-	0.01
Air drag coefficient	C_D		0.35
Front area	A_v	m^2	2.604
Correction coefficient of rotating mass	δ	-	1.04

In this paper, the motor was selected refer to the vehicle demand power calculated by equations (1) - (8), as shown in Table 2. Heat in motor can be generated not only during operation due to iron loss, copper loss, mechanical loss and additional loss [33, 37], but also during recovering the braking energy [25]. Therefore, the motor efficiencies under different torques and revolutions were obtained through experiments as shown in Figure (3), which represents the proportion of the above loss. Figure 4 (a) shows the coupled 3D characteristic cloud map of the motor. The motor heat power P_{mh} can be calculated as equation (9):

$$P_{mh} = P_m(1 - \eta_m) \tag{9}$$

where the P_m is the electrical power of the motor, η_m is the motor efficiency.

Table 2. Specification of the motor

Parameters	Unit	Value
Motor weight	kg	54
Rated power	kW	60
Maximum power	kW	125
Rated torque	Nm	120
Rated revolution	Nm	280
Peak power duration	s	30
Peak torque duration	s	30
Maximum drive current	A	468.2

Maximum generating current	A	470.7
Operating voltage range	V	240-451
Optimal coolant temperature	℃	-40-70

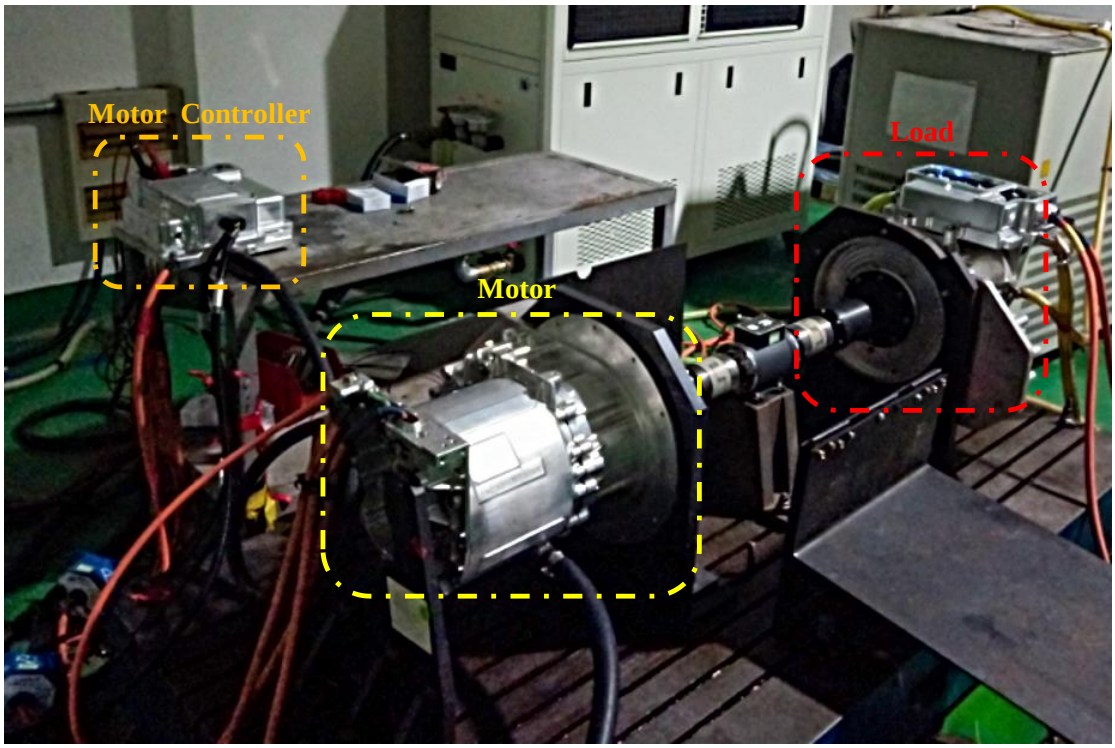

Figure 3. Motor bench test

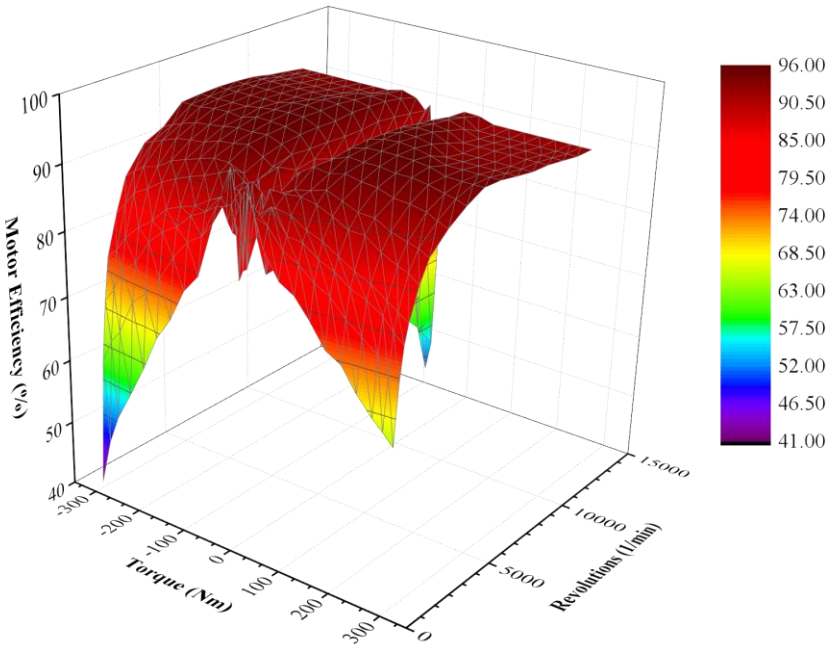

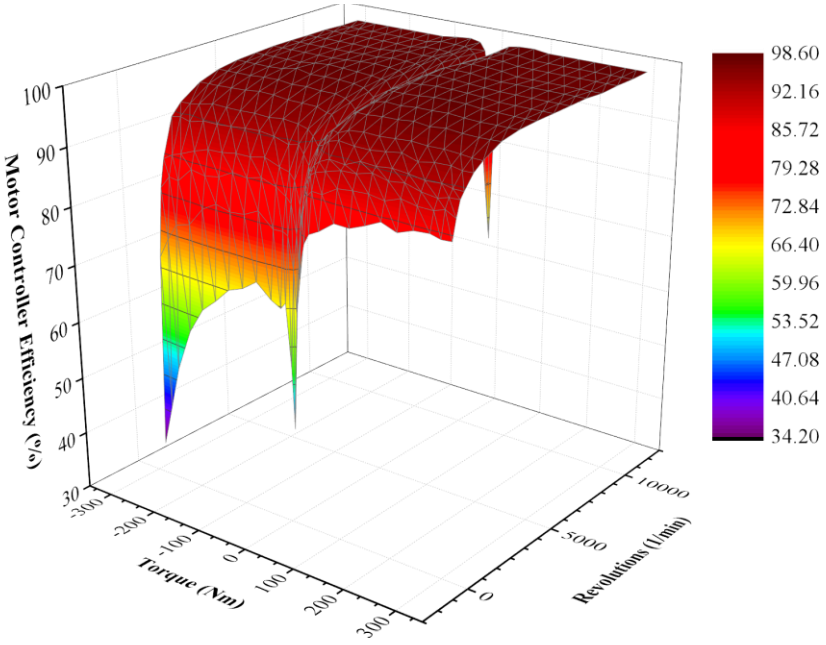

Figure 4. 3D cloud maps of motor efficiency (a) 3D cloud maps of motor controller efficiency (b)

Specification of the motor controller (V0130-60kW) is shown in Table 3. The main heat source of the motor controller comes from the IGBT (Insulated Gate Bipolar Transistor) module which generates enormous amounts of heat during prolonged operation as well as switching on and off frequently. Therefore, the heat power P_{mch} of the motor controller matched with the motor can be calculated as equation (10) and (11):

$$P_{mc} = P_m/\eta_{mc} \tag{10}$$

$$P_{mch} = P_{mc}(1-\eta_{mc}) \tag{11}$$

where P_{mc} is the motor controller input power, η_{mc} is the motor controller efficiency. The data of motor controller efficiency was also obtained through experiment as shown in Figure (3). And then the efficiencies under different torque and revolution are coupled into a 3D characteristic cloud map shown in Figure 4 (b).

Table 3. Specification of the motor controller

Parameters	Unit	Value
Motor controller weight	kg	9.5
Rated power	kW	60
Input voltage range	V	400-750
Speed control range	Hz	0-600
Speed control accuracy	%	±0.02
Torque control accuracy	%	±5
Optimal coolant temperature	℃	-40-65

The heat dissipation of triad (OBC, HJBX and DC/DC) of the electric vehicle was measured in China Automotive Engineering Research Institute Co., Ltd., which was averaged 300W under high-speed condition, WLTC condition and high-speed climbing condition. Therefore, the heat power of OBC, HJBX and DC/DC were regarded as a heat source with a heating power of 300W in this paper.

3.2 Heat transfer

Figure 5 shows the tested thermal exchange power of radiator under various inner coolant volume flow rate and outer air velocity.

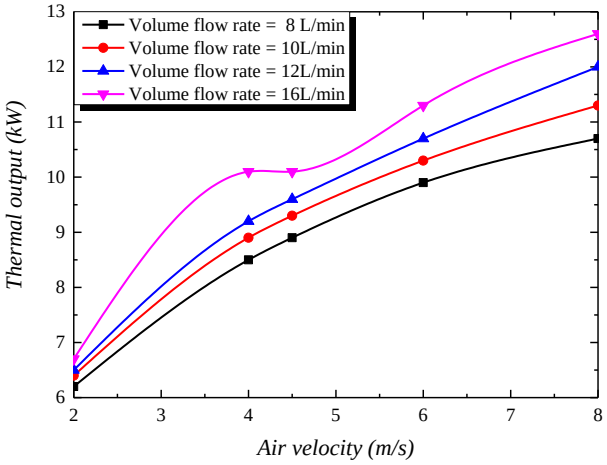

Figure 5. The heat exchange of radiator

Radiator used in this paper is the cross-flow heat exchangers. The heat power P_h of radiator model [10] built in KULI can be calculated as equation (12)-(16) :

$$P_h = \tau P_{ETD} + (1-\tau)P_{\Delta T} \tag{12}$$

$$P_{ETD} = W_k(T_{l(in)} - T_{O(in)})\phi \tag{13}$$

$$P_{\Delta T} = hA(T_{l(mean)} - T_{O(mean)}) \tag{14}$$

$$W_I = \dot{m}_I C_{pI} \tag{15}$$

$$W_O = \dot{m}_O C_{pO} \tag{16}$$

where P_{ETD} is thermal output based on entry temperature difference; W_k is the minimum of W_I and W_O; ϕ is the operation characteristic; $T_{l(in)}$ is the inlet temperature of inner flow; $T_{O(in)}$ is the inlet temperature of outer flow; h is the heat transfer coefficient, A is the heat transfer area, $T_{I(mean)}$ is the mean temperature of inner flow, $T_{O(mean)}$ is the mean temperature of outer flow, $\dot{m}_I$ is the inner mass flow, $\dot{m}_O$ is the outer mass flow, C_{pI} is the specific heat capacity of the inner flow, C_{pO} is the specific heat capacity of the outer flow. The parameter τ depends on the mass flow, $\tau = 1$ for the measure range of the radiator and some extrapolated range, $\tau = 0$ for very small flow rate and $0 < \tau < 1$ (with a smooth transition) in between. In equation (15), the overall heat transfer coefficient h can be expressed by equation (17) and considered as a combination of several heat transfer coefficients, which are heat convection form the outer medium to the structure (α_{OM}), heat conduction through the structure (L/λ_m) and heat convection from the structure to the inner medium (α_{IM}).

$$h = \frac{1}{\frac{1}{\alpha_{OM}} + \frac{L}{\lambda_m} + \frac{1}{\alpha_{IM}}} \tag{17}$$

where L is the material thickness and λ_m is the thermal conductivity of the material. For the α_{OM} and

α_{IM}, they can be calculated as equation (18)-(19):

$$\alpha_{OM} = O_{OM} + C_{OM} Re_{OM} Pr_{OM}^{\frac{1}{3}} \tag{18}$$

$$\alpha_{IM} = O_{IM} + C_{IM} Re_{IM} Pr_{IM}^{\frac{1}{3}} \tag{19}$$

where Re is the Reynolds number; Pr is the Prandtl number which could be obtained by looking up the table. The coefficients O_{OM}, O_{IM}, C_{OM}, C_{IM} are calibrated with the measurement data of the specific component. Re is represented equation (20):

$$R_e = \frac{u_M L_c}{\upsilon} \tag{20}$$

where u_M is the medium velocity; L_c is the characteristic length; υ is the dynamic viscosity.

And the operating characteristic ϕ of a cross-flow heat exchanger, the following expression are given as equation (21)-(24):

$$\begin{cases} \phi = \frac{W_I}{W_O}\left(1 - \frac{1+S}{N} \times e^{-\varepsilon y_0}\right) & W_I > W_O \\ \phi = 1 - \frac{1+S}{N} \times e^{-\varepsilon y_0} & W_I < W_O \end{cases} \tag{21}$$

$$S = \sum_{p=1}^{N-1} \sum_{m=0}^{p} \left(\binom{p}{m} [1 - e^R]^m \times e^{(p-m)R} \sum_{r=0}^{m} \frac{(\varepsilon y_0)^r}{r!}\right) \tag{22}$$

$$\varepsilon y_0 = \frac{W_O}{W_I} \times N \times (1 - e^R) \tag{23}$$

$$R = -\frac{h \times A}{N \times W_O} \tag{24}$$

where N is the number of the tube rows of the heat exchanger.

Temperature of triad, motor controller and motor are increased under operation, the following expression is given as equation (25):

$$Q_{in} = cm\Delta T \tag{25}$$

where Q_{in} is absorbed heat; c is heat capacity; m is weight of component and ΔT is temperature difference of component.

Besides, the cooling of triad, motor controller and motor are based on Newton's law of cooling shown, the following expression is given as equation (26):

$$\phi_s = \alpha_s A_s (T - T_w) \tag{26}$$

where ϕ_s is convective heat transfer rate; α_s is heat transfer rate; A_s is the heat transfer area; T is coolant average temperature and T_w is wall temperature in contact with the fluid.

Besides, since the heat dissipation of triad and motor controller between the pipe and the air is very small, the heat dissipation of the pipe is not considered in this paper. While motor has a larger heat transfer surface in this study, so the heat transfer coefficient h_a of motor is speed-dependent, the following expression is given as equation (27):

$$\begin{cases} h_a = 5.512 + 3.909 * v & v < 5m/s \\ h_a = 7.14 * v^{0.78} & v \geq 5m/s \end{cases} \quad (27)$$

3.3 Model of cooling fan and pump

A fan CL-B101 was adopted as cooling fan in this study, which has three levels: low, medium and high. Volume flow used in this study is the experimental constant value of $1.026m^3/s$ when high, $0.846m^3/s$ when medium and $0.531m^3/s$ when low. And the value of wind pressure was set to 80 Pa according to the fan experiment data. At different modes, the fan supplies different air volumes by consuming electrical energy converted it into mechanical energy for the blades to turn. The greater the air volume, the greater the heat dissipation of the radiator. Therefore, the fan electric power P_{fan}, the following expression is given as equation (28):

$$P_{fan} = \frac{q_{vf} p_{fan}}{3600 * \eta_f * 1000} \quad (28)$$

where q_{vf} is fan volume flow; p_{fan} is wind pressure; η_f is fan efficiency.

A pump P621212D was adopted as water-cooling pump in this study. The pump realized forced convection heat transfer by driving the coolant flow, which takes away heat generated by the electric device during its operation. Besides, the resistance generated by the pipeline, motor controller, motor and triad are overcome by the pump. Therefore, the volume flow q_{vp}, the lift H_m and the electric power P_{pump} of the pump are expressed by equation (29)-(31):

$$q_{vp} = q_t n_p \quad (29)$$

$$H_m = H_0 - S_0 q_{vp}^2 \quad (30)$$

$$P_{pump} = \frac{\rho g q_{vp} H_m}{\eta} \quad (31)$$

where q_t is the pump displacement; n_p is the pump revolution speed; H_0 is the lift of pump at flow of 0 m^3/h, S_0 is the friction within the pump; ρ is the specific gravity of cooling medium; g is the gravitational acceleration; η is the pump efficiency.

Resistance loss of cooling loop is divided into two parts. First part is the along-path resistance loss and local resistance loss generated by the pipeline, the other part is the resistance of the cooling grooves inside the electric devices. In cooling loop of electric drive, there're five parts of the tubes to connect the radiator, triad, motor controller, motor and pump as a loop. The resistance loss ΔP, along-path resistance loss ΔP_1 and the local resistance loss ΔP_2 of every pipeline, the following expression are given as equation (32)-(34).

$$\Delta P = \Delta P_1 + \Delta P_2 \quad (32)$$

$$\Delta P_1 = \lambda \frac{l}{d} \cdot \frac{v^2}{2g} \quad (33)$$

$$\Delta P_2 = \zeta \cdot \frac{v^2}{2g} \quad (34)$$

where λ is the along-path resistance coefficient of the pipeline; ζ is the local resistance coefficient; l is the pipe length; d is the pipe diameter; v is the average velocity of tube section; g is the gravitational acceleration. Since the pipeline is composed of straight and curved pipes with different diameters, the total resistance loss $\sum \Delta P$ of cooling loop of electric drive, the following expression are given as equation (35),

$$\sum \Delta P = \sum (\lambda_i \frac{l_i}{d_i} + \zeta_i) \cdot \frac{v_i}{2g} \tag{35}$$

The physical properties of each section of the pipe were measured according to the 1:1 3D model. In particular, the pipes include five parts in CF, pipe 1—from radiator to the triad (HJBX, DC/DC, OBC), pipe 2—from the triad to motor controller, pipe 3—from motor controller to motor, pipe 4—from motor to water pump and pipe 5—from pump to radiator. In view of the augment of branch lines in IF shown in Figure (3), assume that the pipe between the proportional valve and the motor controller is composed of pipe 1 and pipe 2. In the same way, assuming that the pipe between the proportional valve and the motor is composed of pipe 1, pipe 2 and pipe 3. The triad, motor controller, motor and radiator were experimentally tested and their flow resistance curves were obtained and shown in Figure (6).

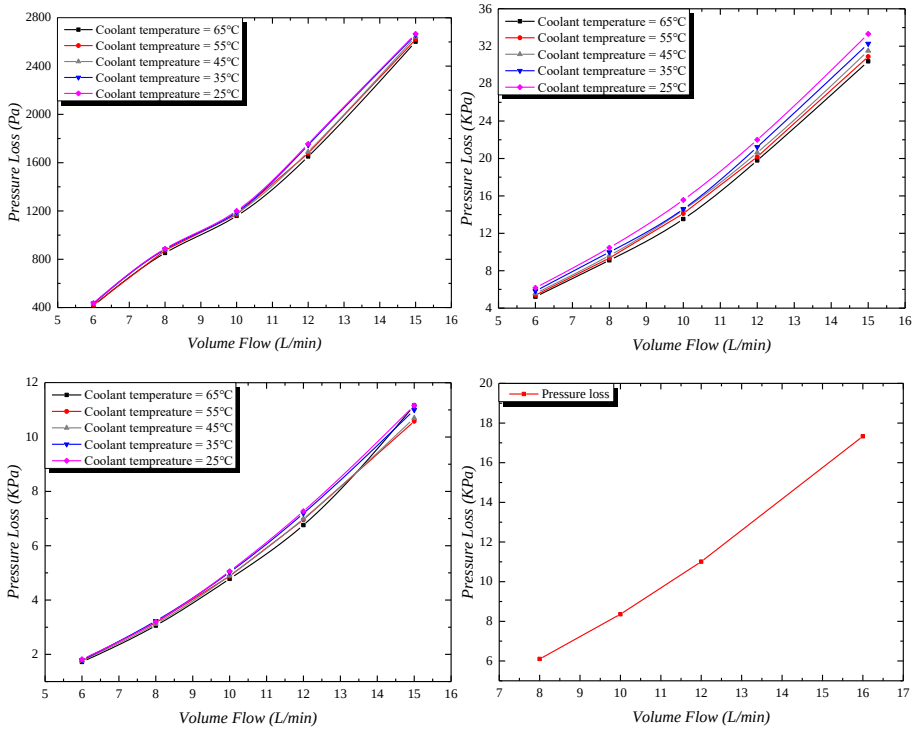

Figure 6. (a) Pressure loss of triad (b) Pressure loss of motor controller (c) Pressure loss of motor at different temperature and mass flow (d) Pressure loss of radiator

3.4 Rule-based control strategies of VTMS

As the generated heat of motor and motor controller model are highly nonlinear and time variant, the rule based control strategies are needed. In this paper, the control strategies are consisted of two parts.

One is used to regulate pump and fan based on signals of the input and output coolant temperature and volume flow of different electric devices. Another is used to adjusted the proportional valve to control the coolant volume flows of different devices. Figure (7) shows control strategies of fan and pump in CF.

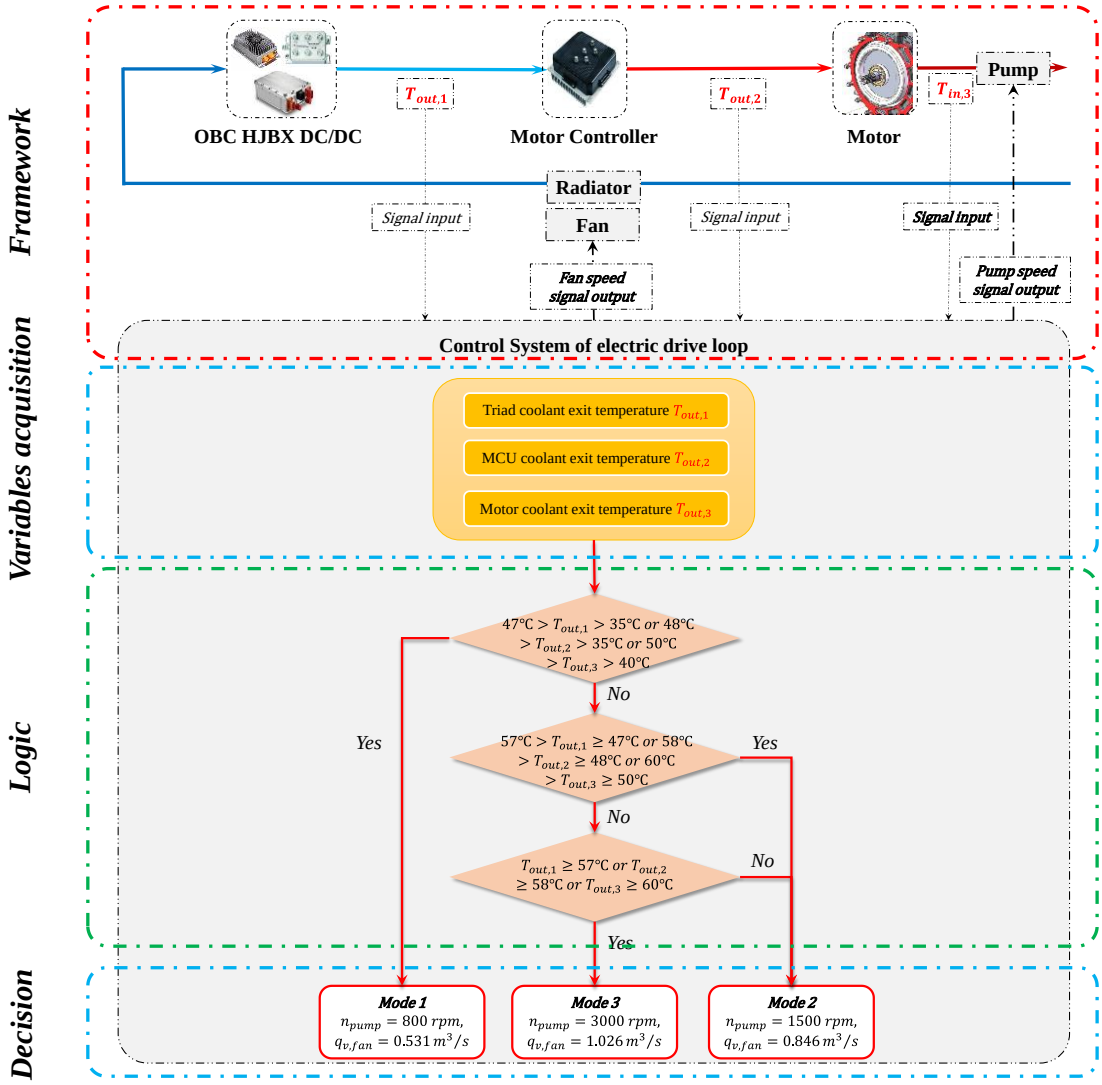

Figure 7. Conventional control strategy of fan and pump

Fan and pump work in mode-switch control strategy which is used in recently produced EVs [8]. Work conditions of fan and pump have 3 modes in this paper. The detailed mode-switch control strategies are shown in Table 4, which are based on the optimal operational temperature requirement of components [8, 38, 39]. Each mode has entry and exit condition that are determined by the coolant outlet threshold temperature of the triad, the motor controller and the motor.

Table 4. Mode-switch control strategies of cooling fan and cooling pump (T_t represents triad outlet temperature, T_{mc} represents motor controller outlet temperature and T_m represents motor outlet temperature)

Mode	Condition	Fan and Pump Status
Mode 1 on	$T_t > 35℃$ *or* $T_{mc} > 35℃$ *or* $T_m > 40℃$	$n_{pump} = 800\ rpm$ $q_{vf} = 0.531\ m^3/s$

Mode 1 off	$T_t < 30℃, T_{mc} < 30℃, T_m < 35℃$	$n_{pump} = 0\ \ rpm$ $q_{vf} = 0\, m^3/s$
Mode 2 on	$T_t > 47℃\ \ or\ \ T_{mc} > 48℃\ \ or\ \ T_m > 50℃$	$n_{pump} = 1500\ \ rpm$ $q_{vf} = 0.846\, m^3/s$
Mode 2 off	$T_t < 45℃, T_{mc} < 46℃, T_m < 48℃$	$n_{pump} = 800\ \ rpm$ $q_{vf} = 0.531\, m^3/s$
Mode 3 on	$T_t > 57℃\ \ or\ \ T_{mc} > 58℃\ \ or\ \ T_m > 60℃$	$n_{pump} = 3000\ \ rpm$ $q_{vf} = 1.026\, m^3/s$
Mode 3 off	$T_t < 55℃, T_{mc} < 56℃, T_m < 58℃$	$n_{pump} = 1500\ \ rpm$ $q_{vf} = 0.846\, m^3/s$

Due to the mode-switch strategies, when any component reaches the threshold temperature, the VTMS system will increase the speed of the pump or fan to enhance heat dissipation. However, increasing cooling ability may be unnecessary to other components, which increases energy consumption of pump and fan. In addition, as temperature drops, so does the mode of pump and fan. Therefore, when driving condition is more complicated, mode changes of pump and fan are more frequent. So, reducing coolant flow in component with low heat dissipation requirements and increasing coolant flow in component with high heat dissipation requirements is necessary, which would help components in cooling loop of electric drive reach threshold temperature almost synchronous. Figure 8 shows strategies of pump, fan and proportional valve in IF. The coolant inlet and outlet temperature, the coolant volume flow and threshold temperature of all components are used to regulate the proportional valve to admeasure volume flow rate.

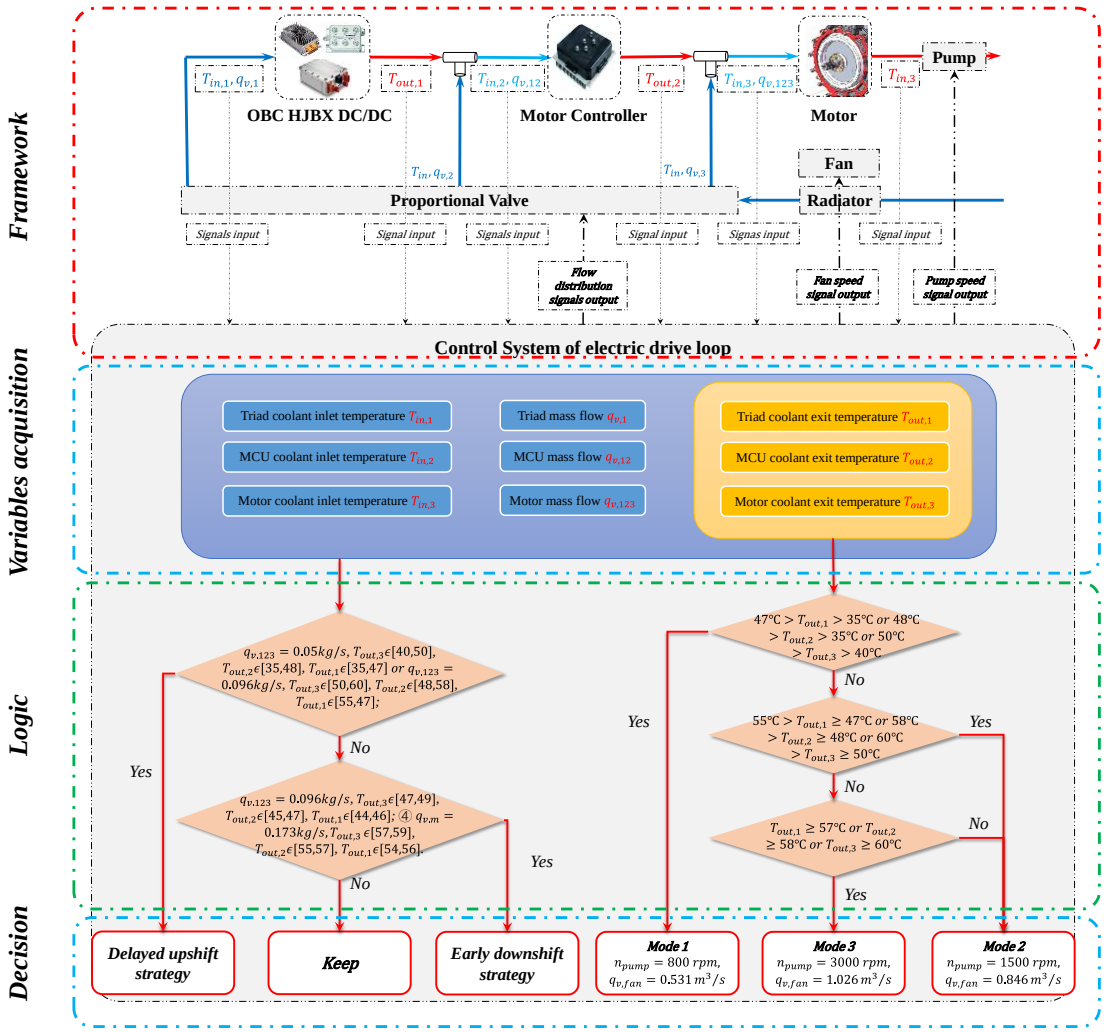

Figure 8. Control strategies of fan, pump and proportional valve

Next, *I*, *J* and *K* are used to represent unknown objects of triad, motor controller or motor. Modes of pump and fan are called *i*. Then the subscript *j* is used to represent the moment. Besides, the subscript t, mc and m represent the triad, motor controller and motor. In order to better regulate the flow distribution, when the coolant outlet temperature of a component approaches a threshold value of upshifting, VTMS recognizes mode *i* of pump and fan, then calculates temperature difference of triad, motor controller and motor ΔT_t, ΔT_{mc} and ΔT_m, which indicates the temperature stability margin of the component, so as to determine the component I that needs the most additional cooling flow by $min(\Delta T_t, \Delta T_{mc}, \Delta T_m)$, which given as equation (36).

$$\begin{cases} \Delta T_t = T_{lim,t,i} - T_{t,o} \\ \Delta T_{mc} = T_{lim,mc,i} - T_{mc,o} \\ \Delta T_m = T_{lim,m,i} - T_{m,o} \end{cases} \tag{36}$$

where $T_{t,o}$ is exit temperature of triad; $T_{mc,o}$ is exit temperature of motor controller; $T_{m,o}$ is exit temperature of motor; $T_{lim,t,i}$, $T_{lim,mc,i}$ and $T_{lim,m,i}$ are threshold value of triad, motor controller and motor under mode *i*, respectively.

The coolant heat exchange $Q_{J,j}$ and $Q_{K,j}$ of *J* and *K* at the moment of *j* can be calculated as equation (37) and (38),

$$Q_{J,j} = cq_{m,J,j}(T_{J,out,j} - T_{J,in,j}) \tag{37}$$

$$Q_{K,j} = cq_{m,K,j}(T_{K,out,j} - T_{K,in,j}) \tag{38}$$

where $q_{m,J,j}$ and $q_{m,K,j}$ are the mass flow rate of *J* and *K* at the moment of *j*; $T_{J,out,j}$, $T_{J,in,j}$, $T_{K,out,j}$ and $T_{K,in,j}$ are the inlet and outlet temperature of *J* and *K* at the moment of *j* respectively.

Assuming that the heat transfer at *j+1* is the same as at *j*, then the coolant flow $q_{m,J,j+1}$, $q_{m,K,j+1}$ of the other two components *J* and *K* can be calculated as equation (39) and (40),

$$q_{m,J,j+1} = \frac{Q_{J,j}}{c(T_{lim,J,i} - \eta*(T_{lim,J,i} - T_{J,out,j}) - T_{J,in,j})} \tag{39}$$

$$q_{m,K,j+1} = \frac{Q_{K,j}}{c(T_{lim,K,i} - \eta*(T_{lim,K,i} - T_{K,out,j}) - T_{K,in,j})} \tag{40}$$

where η is a dimensionless coefficient, $0 < \eta < 1$. The closer η is to 0, the more heat is transferred from *I* to *J* and *K* at *j+1*. And the closer η is to 1, the less heat is transferred.

Considering that the cooling flow is merged in the loop, it means that reducing the flow of the front component will increase the inlet temperature of the rear component, which may cause the outlet temperature of the rear component to exceed the threshold. Therefore, the increased mass flow $q_{m,I,j+1}$ of *I* at *j+1* is calculated as equation (41) – (43),

$$q_{m,I,j+1} = q_{m,I,j} + \frac{1}{2}*(\Delta q_{m,J} + \Delta q_{m,K}) \tag{41}$$

$$\Delta q_{m,J} = q_{m,J,j} - q_{m,J,j+1} \tag{42}$$

$$\Delta q_{m,K} = q_{m,K,j} - q_{m,K,j+1} \tag{43}$$

And the decreased mass flow $q'_{m,J,j+1}$ and $q'_{m,K,j+1}$ at *j+1* are calculated as equation (44) and (45),

$$q'_{m,J,j+1} = q_{m,J,j} - \frac{1}{2} * \Delta q_{m,J} \tag{44}$$

$$q'_{m,K,j+1} = q_{m,K,j} - \frac{1}{2} * \Delta q_{m,K} \tag{45}$$

At last, the proportional distribution values $x_{1,j+1}$, $x_{2,j+1}$ and $x_{3,j+1}$ of the flow rate of the proportional valve are calculated as equation (46) – (51),

$$x_{1,j+1} = x_{1,j} - p * \Delta x_1 \tag{46}$$

$$x_{2,j+1} = x_{2,j} - p * \Delta x_2 \tag{47}$$

$$x_{3,j+1} = x_{3,j} - p * \Delta x_3 \tag{48}$$

$$\Delta x_1 = \frac{q_{m,I,j} - q_{m,I,j+1}}{q_{m,K,j}} \tag{49}$$

$$\Delta x_2 = \frac{q_{m,J,j} - q'_{m,J,j+1}}{q_{m,K,j}} \tag{50}$$

$$\Delta x_3 = \frac{q_{m,K,j} - q'_{m,K,j+1}}{q_{m,K,j}} \tag{51}$$

where *p* is the proportional gain.

3.5 Co-simulation model

In this paper, the co-simulation of KULI and Simulink was adopted in this paper. KULI is used to solve complex heat dissipation and energy consumption calculation of this system, while Simulink is used to identify system stage and control pump, fan and proportional valve.

In this study, all physical models derived from a commercial electric vehicle were established in KULI based on experiment data, including the MAP of motor and motor controller (Figure 4), the heating power of triad under different test conditions, the head, efficiency and power of the water pump, the air supply and power of the fan (Table 4), the heating dissipation power of radiator (Figure 5), and the flow resistance of all components (Figure 6) and every pipeline. Then all the components are connected to each other according to the framework of the VTMS to form cooling loop of electric drive shown in Figure (9). However, due to the trade secret information involved, more detailed parameter information and experimental data cannot be disclosed.

On the other hand, control models of pump, fan and proportional valve were connected through SL module in KULI. Detailed strategies shown in table (4) and Figure (7) and (8) were devised based on classified control strategies of multiple EVs and several references [8, 10, 33, 38].

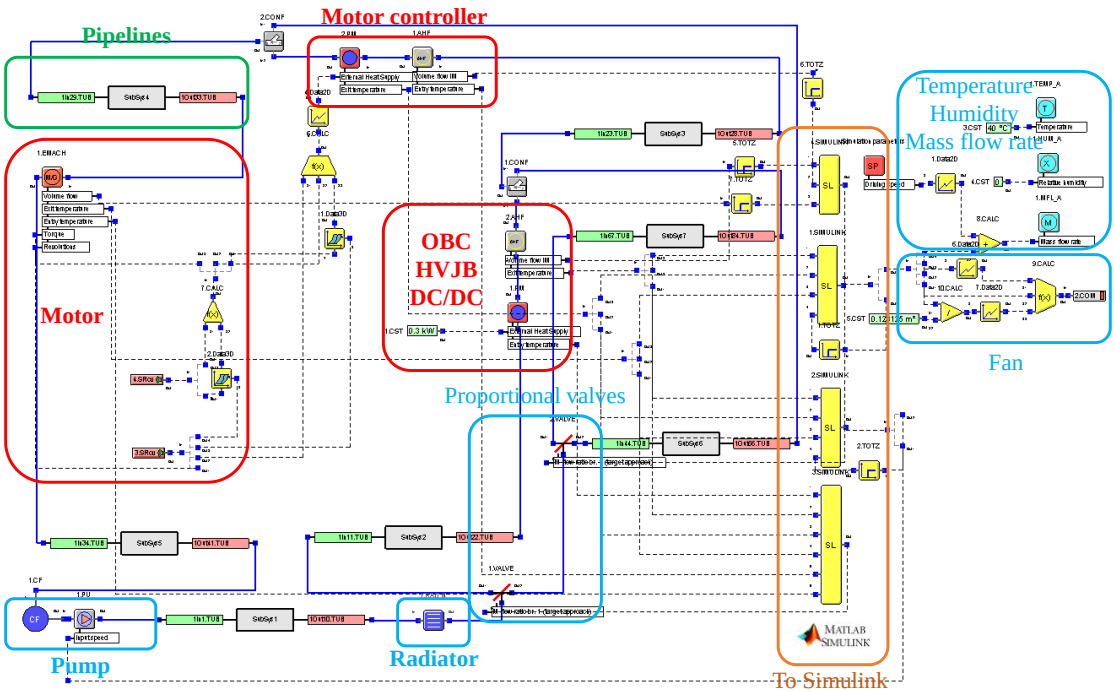

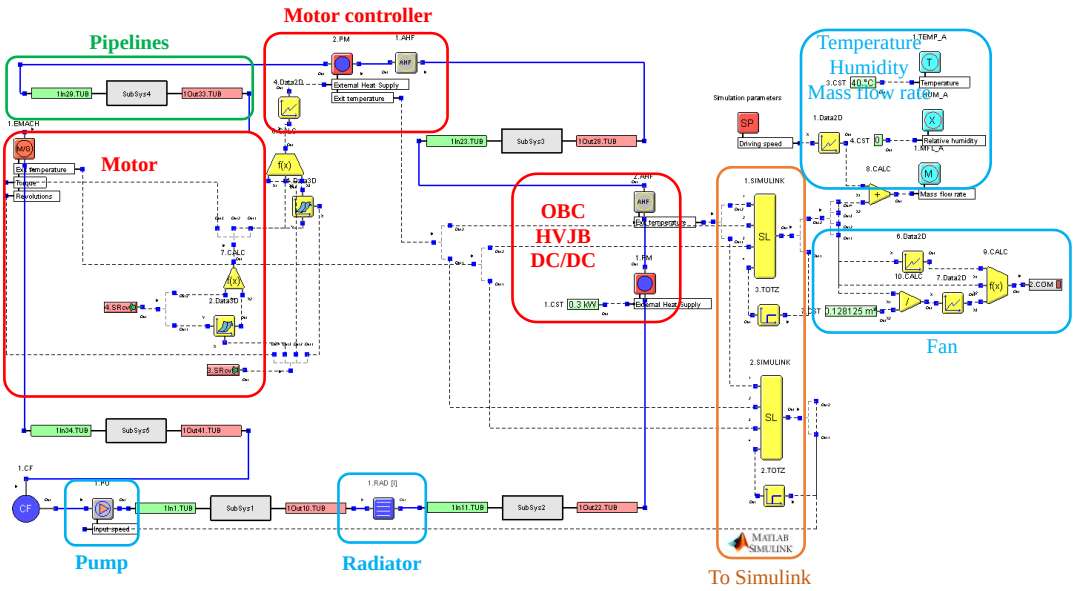

Figure 9. Conventional framework (a) and Innovative framework (b) models in KULI

4. Results and discussion

4.1 Model validation

In this study, VTMS model was validated by experimental results of climbing condition (climbing angle is 9º, ambient temperature is 40 ºC, inlet temperature of radiator is exit temperature of condenser due to a different VTMS framework, coolant flow rate is in the range of 9.3-9.8L/min). The experimental results are derived from another EV which combines OBC, HVJX, DCDC and motor controller. Then, Figure (10) shows errors of motor controller (plus triad), motor and radiator between experimental results and simulation results.

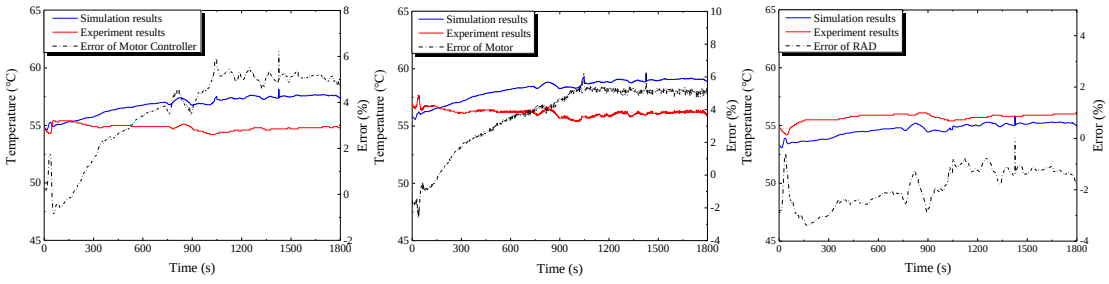

Figure 10. Error (%) of VTMS simulation model (a) Triad and motor controller, (b) motor, (c) radiator

From Figure (10), errors for triad and motor controller is in the range of -0.9~6.29%. In addition, errors for motor and radiator are in the range of -2.64~6.34% and -3.4~0.07%. The above data shows that VTMS model in this study is rational.

4.2 Steady-stage simulation

To compare the thermal management performance under three extreme high temperature conditions: highest speed, high-speed climbing and low-speed climbing, the steady-stage simulation was conducted for two electric drive thermal management framework. Steady-stage conditions parameters are shown in Table 5. The heat generated by the motor and motor controller depend on the intensity of condition. High speed and climbing undoubtedly increase the load of the motor, but high speed also brings more air intake to the radiator. In addition, compared with CF of cooling loop of electric drive, the added pipelines in IF have a smaller flow resistance due to less passing triad and motor controller, which indirectly increases the flow without increasing the pump speed. Modes of pump and fan are controlled by the identical control strategies.

Table 5. Steady-stage conditions parameters

Conditions	Speed (km/h)	Slope	Ambient pressure (kPa)	Ambient Temperature (°C)	Air humidity (%)
Highest speed	120	0	101.3	40	50
High-speed climbing	90	0.03	101.3	40	50
Low-speed climbing	50	0.08	101.3	40	50

According to the results from table 6, both frameworks have the ability to meet the cooling requirements of components. The maximum permissible coolant temperature of motor controller and motor could be checked from table 2 and table 3. Besides, the maximum permissible coolant temperature of OBC, HVJB and DC/DC are set to 65°C, which shown in their instructions and reference [35]. Apparently, the inlet and outlet temperatures of components in the IF are lower than the conventional ones. According to Equations (12) - (24), air flow and coolant flow increase the heat exchange ability. Due to the same simulation conditions, the heating power, the air flow and the speed of pump of two frameworks share the same values. Therefore, the IF has a better thermal management performance.

Table 6. Results of steady-stage simulations of CF

Conditions	Framework	Triad entry temperature (°C)	Triad exit temperature (°C)	Controller entry temperature (°C)	Controller exit temperature (°C)	Motor entry temperature (°C)	Motor exit temperature (°C)	Valve 1 flow ratio (%)	Valve 2 flow ratio (%)
Highest speed	Conventional	53.09		53.59		54.09	58.79	-	-
	Innovative	48.86	52.05	50.54	52.20	49.49	52.70	10	10
High-speed climbing	Conventional	56.11		56.60		57.48	62.67	-	-
	Innovative	51.95	55.15	53.32	55.80	52.86	56.45	10	15
Low-speed climbing	Conventional	48.34		49.09		50.02	53.20	-	-

Innovative	44.44	46.24	45.67	47.20	45.65	48.15	30	20

Working modes of pump and fan are set as 3 under highest speed (HS) and high-speed climbing (HSC) condition. The exit temperature of IF under HS and HSC condition is lower than the exit temperature of CF. Although the proportional valve admeasures 76.5% of the flow to motor, the exit temperature of traid and motor controller of IF are also lower than the exit temperature of CF. And the lower exit temperature of motor is achieved by proportional valve. The convective heat transfer mechanism, equation (25) shows that the greater the temperature difference between the cooling fluid and the cooled object, the better the heat transfer effect will be without changing the flow rate. Moreover, working modes of pump and fan are set as 2 under low-speed climbing (LSC) condition. And exit temperature of IF under LSC condition is also lower than exit temperature of CF.

It's worth noting that VTMS recognizes that the exit temperature of IF under HS and HSC condition is in mode 2 based on Table (4). If modes of pump and fan are set as 2, VTMS recognizes that the exit temperature is in mode 3 under HSC condition and mode 2 under HS condition. Therefore, modes of pump and fan of IF under HSC condition switch back and forth between mode 2 and 3 instead of staying mode 3 like CF. Therefore, IF reduces energy consumption of pump and fan (fan consumes 135W and pump consumes 1.2W in mode 1, fan consumes 227W and pump consumes 9.5W in mode 2, fan consumes 312W and pump consumes 24.5W in mode 3).

~~Therefore, these simulation results show that IF not only improves thermal management performance of cooling loop of electric drive of VTMS, but also helps to reduce energy consumption of pump and fan.~~

4.3 Transient simulation

CF model and IF model adopted transient simulations under worldwide harmonized light vehicles test cycle (WLTC) condition, highway fuel economy test (HWFET) cycles and US06 cycle respectively, to compare the difference and investigate the control performance of strategies [40]. Four speed ranges of low, medium, high and extra high are consisted in the Class 3a cycle of WLTC which replaced the new European driving cycle (NEDC) based procedure for type approval testing of light-duty vehicles [41]. The HWFET is used to determine the highway fuel economy rating. In addition, the US06 Supplemental Federal Test Procedure (SFTP) is developed to address the shortcomings with the FTP-75 test cycle in the representation of aggressive, high speed and/or high acceleration driving behavior, rapid speed fluctuations, and driving behavior following startup. Vehicle speed-time curves of cycles were shown in Figure 11, where the blue lines represent two WLTC cycles, the red lines represent 5 HWFET cycles and the green lines represent 6 US06 cycles. Besides, the ambient temperature is 40 ^{o}C, the atmospheric pressure is 101.3kPa and the relative humidity is 50%. Figure (12)-(15) show results of transient simulations.

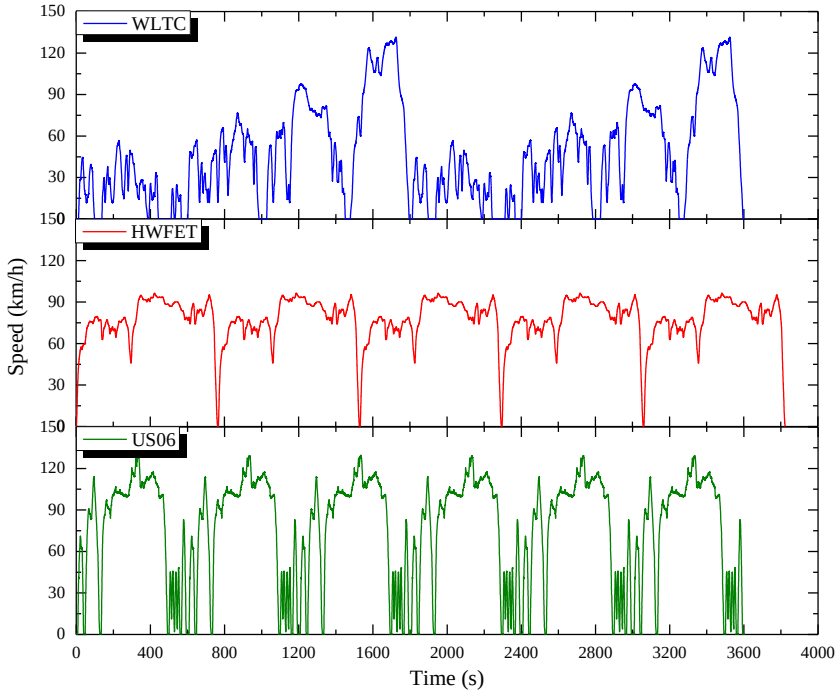

Figure 11. Speed curves of the WLTC, HWFET and US06

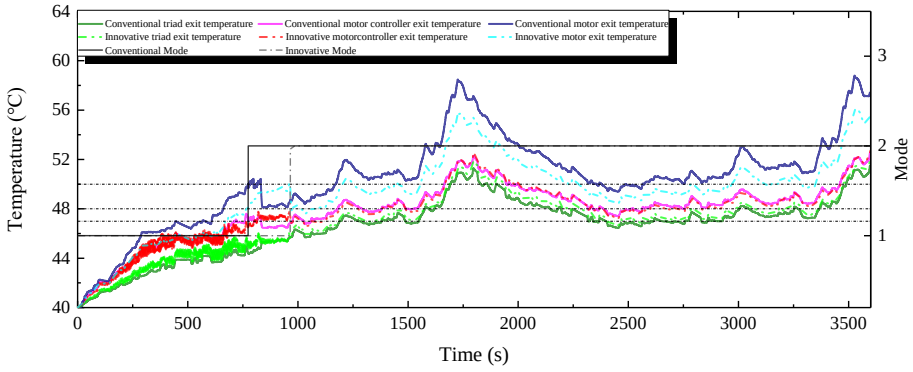

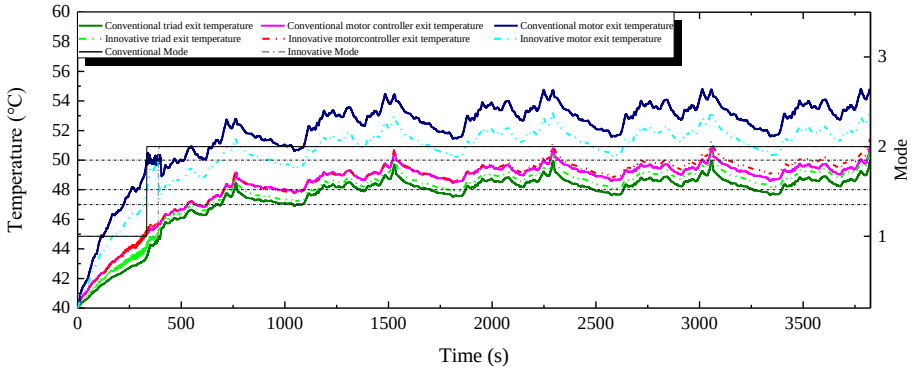

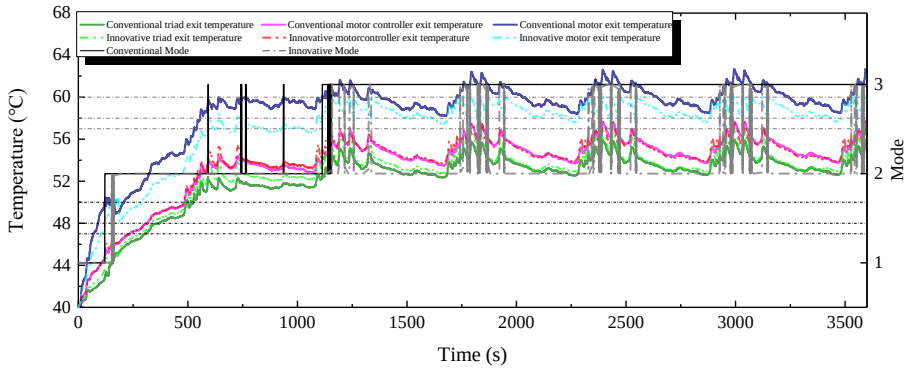

Figure 12. Cooling performance comparison of two frameworks (a) under WLTC, (b) under HWFET, (c) under US06

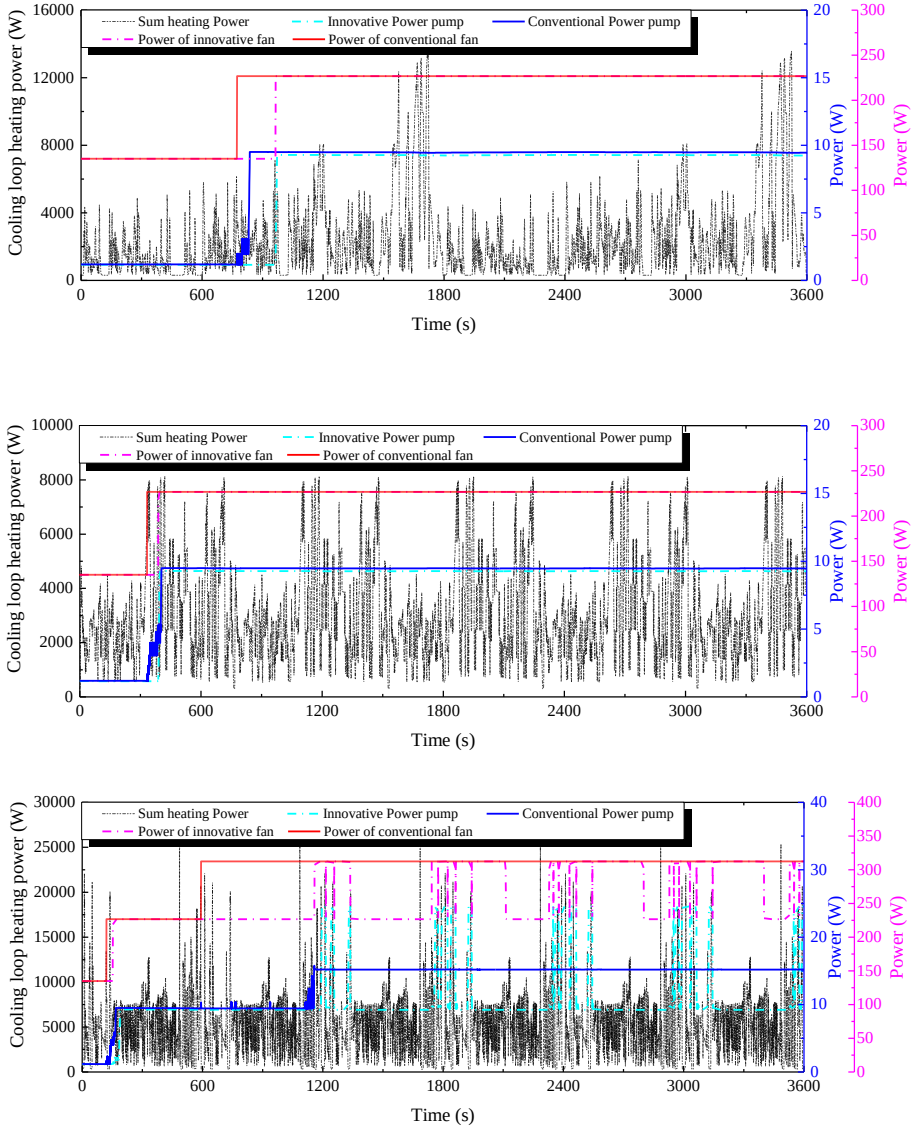

Figure 13. Heating power and cooling power of two frameworks (a) under WLTC, (b) under HWFET, (c) under US06

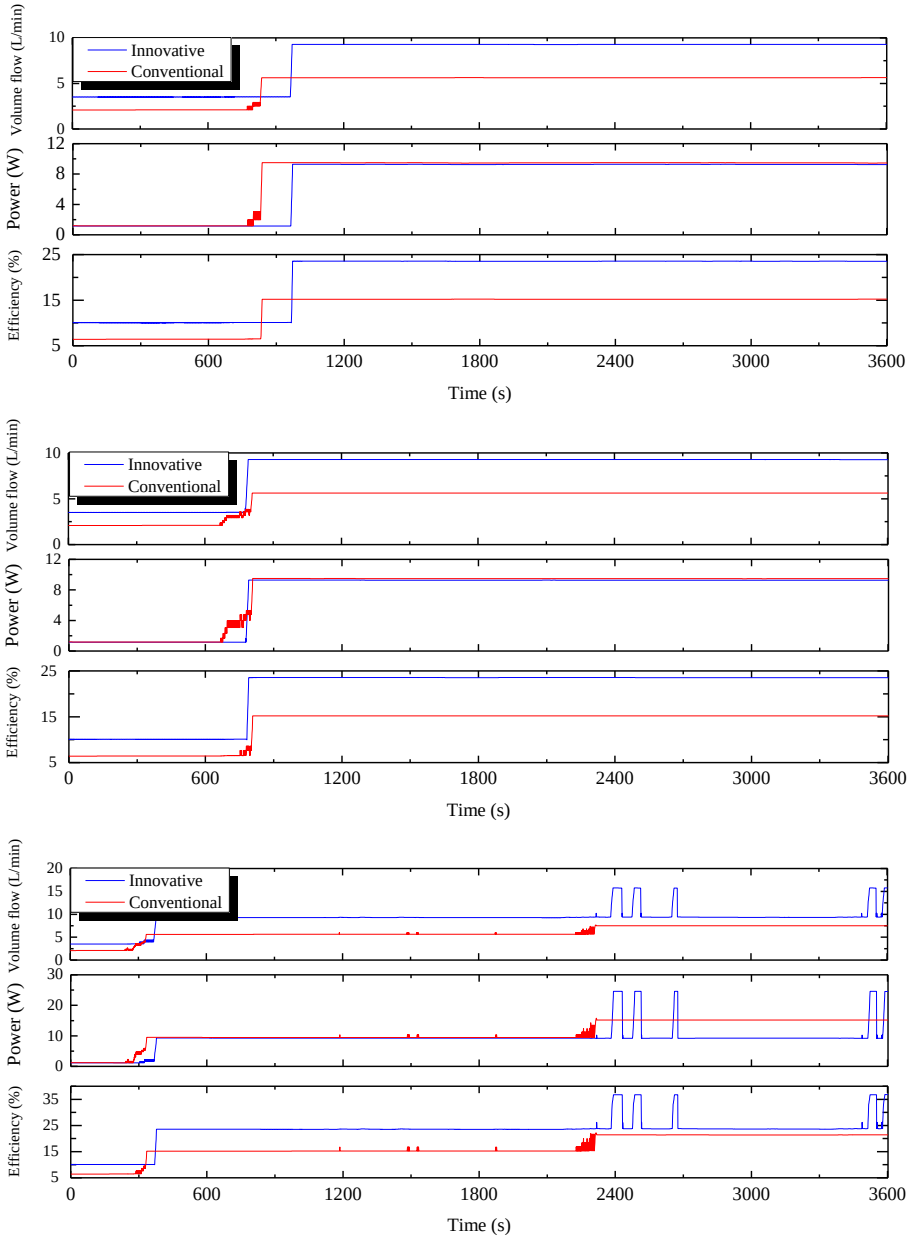

Figure 14. Fan volume flow, power and efficiency of two frameworks (a) under WLTC, (b) under HWFET, (c) under US06

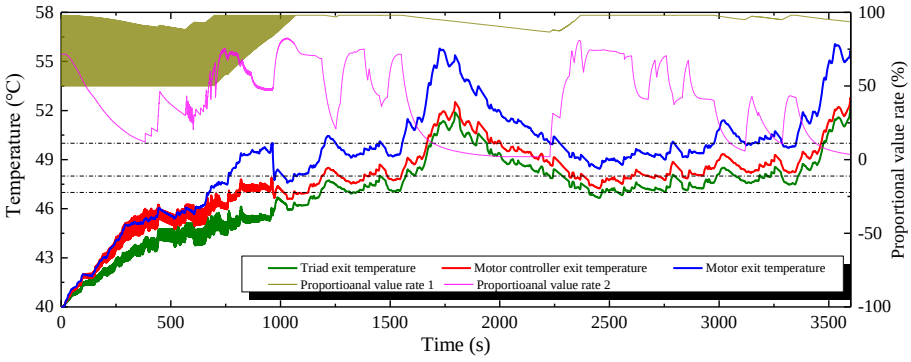

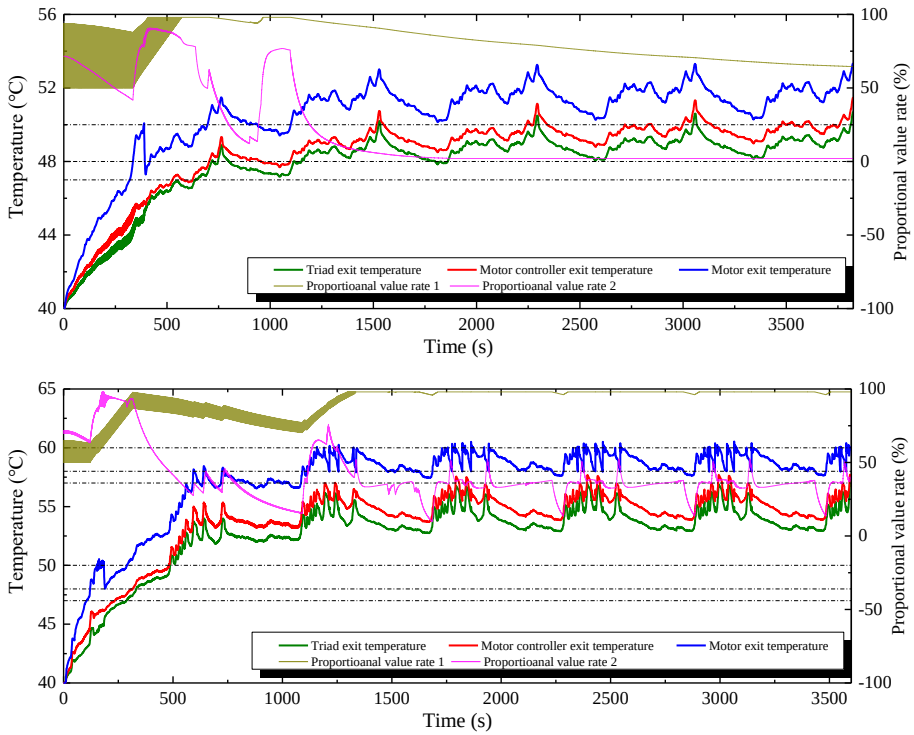

Figure 15. Proportional valve changes of innovative framework (a) under WLTC, (b) under HWFET, (c) under US06

From Figure (12), exit temperature of the motor and motor controller of IF is lower than that of the CF under WLTC, HWFET and US06 condition, while exit temperature of the triad is slightly higher. Compared with CF, the exit temperature of IF was 1.12 ºC lower on average in WLTC condition, 1.49 ºC lower on average in HWFET condition, 1.46 ºC lower on average in US06 condition. In addition, combined with thresholds (black dash dot lines in Figure 12, 15) of triad, motor controller and motor in Table (4), it can be seen that IF postponed time to reach the threshold. Mode of pump and fan in IF changed from 1 to 2, with a delay of 190s under WLTC condition, a delay of 55.5s under HWFET condition and a delay of 31.5s under US06 condition. In addition, the statistical results of Figure 12 (c) show that mode 3 lasts 2494s under CF and 490.5s under IF, which reflected better thermal management performance of IF.

Figure (13) shows the power variations of the cooling fan and cooling pump under the two frameworks at the same heat generating power. On the one hand, it's obvious that mode switch of VTMS is delayed. On the other hand, power consumption of pump is slightly reduced due to a promoted efficiency.

In fact, the revolution of water pump is set as 800rpm, 2000rpm and 3000rpm in modes 1, 2 and 3, respectively. However, Figure (14) show that the cooling volume flow and efficiency of the water pump of IF are significantly higher than that of CF, while the power consumption of pump is slightly lower than that of CF except mode 3. Although model 3 of IF increased pump power by 38%, it also increased volume flow by 52%. Therefore, IF can increase the pump energy efficiency and volume flow under the same mode. In particular, pump and fan reduce energy consumption by 13.4% (1374.4J), 5.2% (17525.4J) under a single WLTC cycle (1802s), 4.1% (169.0J), 3.5% (5046.6J) under a single HWFET cycle (765s), 7.6% (334.6J) and 2.8% (3533.2J) under a single US06 cycle (600s). It is worth noting that energy consumption of pump and fan was reduced by 19.3% and 12.0% respectively under 6 US06 cycle conditions (3600s).

Mode switch of CF is caused by the motor first reaching the threshold of 50 ºC in Figure 12 (a), (b)

and (c), which indicates that the motor had a greater demand for heat dissipation under the current working condition. Figure (15) shows two proportional valves rates changes and exit temperature of triad, motor controller and motor in IF. The larger the value of proportional valve 1 indicates that the VTMS allocates more flow to triad which has higher heat dissipation requirement. And value of proportional valve 2 is the same. (Due to the limitations of model of KULI software, two two-port proportional valve models were used instead of a three-port proportional valve. Where the proportional valve 1 represented the flow proportion allocated to the triad, and the proportional valve 2 represented the flow proportion allocated to the motor controller. It should be noted that the flow allocated by the proportional valve 2 is the difference of the total flow and the flow allocated to triad.) With the augment of heating power, the control strategy of proportional valve adjusted the flow distribution so that the triad, motor controller and motor were synchronized close to their respective thresholds, which delayed the time when the electric drive circuit reaches the threshold of mode-switch.

In those simulation conditions, only the US06 condition enables the fan and pump to reach mode 3, which indicates that the thermal management system of this electric vehicle can control the outlet temperature of the motor below 60 ºC as long as it is not driven fiercely even under extremely high temperature conditions. However, according to the value of proportional valve 1 in Figure (15), VTMS allocates more than 90% of the coolant flow to the triad except for the HWFET condition. Compared with the transient condition, it can be seen that the proportional valve have a wider range of flow regulation under the steady-state condition, which indicates that the proportional valve could work better in continuous high power motor. Moreover, Figure (15) shows that at the beginning of the cycle, the proportional valve 1 has a large oscillation, which occurs when the load changes dramatically and modes of pump and the cooling fan are too low. In addition, there is no typical mode downshift comparison in three working conditions to testify downshift strategies of proportional valve. It is all about the high ambient temperature leads to small temperature difference between the outer air and the inner coolant. Therefore, VTMS need toto maintain or increase $\dot{m}$ to maintain or increase W_O, thereby increasing W_k (when $W_O < W_I$) or ϕ (when $W_O > W_I$), and finally supplementing the heat dissipation power of radiators.

5. Conclusion

Two cooling loop framework of electric drive of VTMS and the corresponding control strategies were established in this paper. Thermal management performance and the energy consumption level of water pump and cooling fan of two frameworks were compared and studied by KULI/Simulink co-simulation. Two frameworks adopted the same mode-switch control strategies for pump and fan. In addition, a proportional valve and a matching control strategy of IF were used to control the cooling flow through the triad, motor controller, and motor. The main conclusions are summarized as following:

(1) The innovative method of VTMS can tremendously enhance thermal management performance of cooling loop of electric drive. On the one hand, steady-stage simulation results showed that the maximum outlet temperature of triad, motor controller and motor were 56.60 ºC, 57.48 ºC and 62.67 ºC in CF, while the maximum outlet temperature of triad, motor controller and motor were 55.15ºC, 55.80 ºC and 56.45 ºC in IF. On the other hand, from transient simulation results,

it can be seen that exit temperature of the IF was 1.12 ºC lower on average in 2 WLTC cycles, 1.49 ºC lower on average in 5 HWFET cycles and 1.46 ºC lower on average in 6 US06 cycles.

(2) The addition of proportional valves and matched control strategy enabled refined thermal management of the drive circuit components. All components reach thresholds almost at the same time, which caused that VTMS postponed the upshift time of pump and fan of 190s under WLTC cycle, 55.5s of HWFET cycle, 31.5s of US06 cycle.

(3) Energy consumption of fan and pump is reduced. In particular, pump and fan reduce energy consumption by 13.4% (1374.4J), 5.2% (17525.4J) under a single WLTC cycle, 4.1% (169.0J), 3.5% (5046.6J) under a single HWFET cycle, 7.6% (334.6J) and 2.8% (3533.2J) under a single US06 cycle.

(4) Augment of pipes lead to increased pump efficiency. The increase in the pipeline increases the pump efficiency from 6.41% to 10.1% in mode 1, from 15.2% to 23.6% in mode 2, and from 21.4% to 36.8% in mode 3.

6. Acknowledgments

This work is supported in part by the National Key Research and Development Program (No.: 2018YFB0105702), the Technological Innovation and Application Demonstration in Chongqing (Major Themes of Industry: cstc2018jszx-cyztzxX0005, cstc2019jscx-zdztzxX0033), and the Fundamental Research Funds for the Central Universities (No.: 2019CDXYQC0003, No.: 244005202014, and No.: 2018CDXYTW0031).This work is also supported by Magna PT Powertrain (Shanghai) Co., Ltd., for providing KULI technical service. M. Ni thanks the grants (Project Number: PolyU 152214/17E and PolyU 152064/18E) from Research Grant Council, University Grants Committee, Hong Kong SAR.

7. References

[1] Kwon C, Kim MS, Choi Y, Kim MSJIJoR-rIDF. Performance evaluation of a vapor injection heat pump system for electric vehicles. 2017;74:138-50.

[2] Xia GD, Cao L, Bi GJJoPS. A review on battery thermal management in electric vehicle application. 2017;367:90-105.

[3] Zhang Y, Zhang C, Huang Z, Xu L, Liu M. Real-Time Energy Management Strategy for Fuel Cell Range Extender Vehicles Based on Nonlinear Control. 2019.

[4] Kandidayeni M, Macias A, Boulon L, Energy SKJA. Investigating the impact of ageing and thermal management of a fuel cell system on energy management strategies. 2020;274:115293.

[5] Li M, Bai Y, Zhang C, Song Y, Jiang S, Grouset D, et al. Review on the research of hydrogen storage system fast refueling in fuel cell vehicle. 2019;44:10677-93.

[6] a RF, a CZ, b YW, c CJ, b ZM, b LX, et al. Numerical study on the effects of battery heating in cold climate.26.

[7] Jouhara H, Khordehgah N, Serey N, Almahmoud S, Lester SR, Machen D, et al. Applications and thermal management of rechargeable batteries for industrial applications. 2019;170:849-61.

[8] Wang Q, Liang D, Wang J. Electric vehicle self-adaptive energy-saving cooling system design based on fuzzy control methods of fan and pump electromotors. international conference on ecological vehicles and renewable energies2015. p. 1-4.
[9] Xia Y, Zhang Z, Wu Y, Li Y. INTELLIGENT MULTI-LOOP THERMAL MANAGEMENT SYSTEM FOR AN ELECTRIC VEHICLE. 2018.
[10] Xu J, Zhang C, Fan R, Bao H, Energy CLJ. Modelling and control of vehicle integrated thermal management system of PEM fuel cell vehicle. 2020:117495.
[11] Zhang G, Zou H, Qin F, Xue Q, Tian CJATE. Investigation on an improved heat pump AC system with the view of return air utilization and anti-fogging for electric vehicles. 2017;115:726-35.
[12] Kondo T, Katayama A, Suetake H, Morishita M. Development of Automotive Air-Conditioning Systems by Heat Pump Technology.
[13] Danca P, Vartires A, Dogeanu AJEP. An Overview of Current Methods for Thermal Comfort Assessment in Vehicle Cabin. 2016;85:162-9.
[14] Bracco R, Seccardini R, Somma MD, Gallardo G, Fabio SJTRP. CONVENIENT – Complete Vehicle Energy Saving Technologies for Heavy Trucks. 2016;14:1041-50.
[15] Engineering AJA. Electric vehicle drive systems. 1998.
[16] Lan S, Yang Z, Chen R, Stobart RJAE. A dynamic model for thermoelectric generator applied to vehicle waste heat recovery. 2018;210:327-38.
[17] Shabashevich A, Richards N, Hwang J, Erickson PAJAE. Analysis of powertrain design on effective waste heat recovery from conventional and hybrid electric vehicles. 2015;157:754-61.
[18] c XHab, a HZ, a JW, c CTa, a MT, Energy GHacJR. Investigation on the heating performance of the heat pump with waste heat recovery for the electric bus. 2020;152:835-48.
[19] a PD, b ZW, a YW, Energy KLaJR. A distributed multiple-heat source staged heating method in an electric vehicle. 2020;150:1010-8.
[20] Wang Y, Li W, Zhang Z, Shi J, Chen JJATE. Performance evaluation and prediction for electric vehicle heat pump using machine learning method. 2019;159:113901.
[21] Liu C, Zhang Y, Gao T, Shi J, Chen J, Wang T, et al. Performance evaluation of propane heat pump system for electric vehicle in cold climate. 2018;95:51-60.
[22] Bellocchi S, Guizzi GL, Manno M, Salvatori M, Zaccagnini AJATE. Reversible heat pump HVAC system with regenerative heat exchanger for electric vehicles: Analysis of its impact on driving range. 2018;129:290-305.
[23] Zhou G, Li H, Liu E, Li B, Yan Y, Chen T, et al. Experimental study on combined defrosting performance of heat pump air conditioning system for pure electric vehicle in low temperature. 2017;116:677-84.
[24] Jiang L, Wang RZ, Li JB, Wang L, Roskilly APJEC, Management. Performance analysis on a novel sorption air conditioner for electric vehicles. 2018;156:515-24.
[25] Ahn JH, Kang H, Lee H, Kim YCJAE. Performance characteristics of a dual-evaporator heat pump system for effective dehumidifying and heating of a cabin in electric vehicles. 2015;146:29-37.
[26] Fan C, Yan G, Yu JJATE. Thermodynamic analysis of a modified solar assisted ejector-compression heat pump cycle with zeotropic mixture R290/R600a. 2019;150:42-9.
[27] Zhu C, Lu F, Zhang H, Mi CCJIJoE, Electronics STiP. Robust Predictive Battery Thermal Management Strategy for Connected and Automated Hybrid Electric Vehicles Based on

Thermoelectric Parameter Uncertainty. 2018;6:1796-805.
[28] Lopezsanz J, Ocampomartinez C, Alvarezflorez J, Morenoeguilaz M, Ruizmansilla R, Kalmus J, et al. Nonlinear Model Predictive Control for Thermal Management in Plug-in Hybrid Electric Vehicles. 2017;66:1-.
[29] Wang Y, Gao Q, Zhang T, Wang G, Jiang Z, Li YJE. Advances in Integrated Vehicle Thermal Management and Numerical Simulation. 2017;10:1636.
[30] Zhang G, Kandlikar SGJIJoHE. A critical review of cooling techniques in proton exchange membrane fuel cell stacks. 2012;37:2412-29.
[31] Zhang F, Gerada D, Xu Z, Zhang X, Tighe C, Zhang H, et al. Back-iron Extension Thermal Benefits for Electrical Machines with Concentrated Windings. 2019:1-.
[32] Nategh S, Krings A, Wallmark O, Leksell MJITotIE. Evaluation of Impregnation Materials for Thermal Management of Liquid-Cooled Electric Machines. 2014;61:5956-65.
[33] Yang Y, Bilgin B, Kasprzak M, Nalakath S, Sadek H, Preindl M, et al. Thermal management of electric machines. 2017;7:104-16.
[34] Li K, Yan J, Chen H, Wang QJATE. Water cooling based strategy for lithium ion battery pack dynamic cycling for thermal management system. 2018:575-85.
[35] Park HJIJoH, Transfer M. Numerical assessment of liquid cooling system for power electronics in fuel cell electric vehicles. 2014;73:511-20.
[36] Tao, Zeng, Caizhi, Zhang, Minghui, Hu, et al. Modelling and predicting energy consumption of a range extender fuel cell hybrid vehicle. 2018.
[37] Sun Y, Zhang S, Yuan W, Tang Y, Li J, Tang KJATE. Applicability study of the potting material based thermal management strategy for permanent magnet synchronous motors. 2019;149:1370-8.
[38] Alaawar N, Arkadan AAJIJoE, Electronics STiP. Optimal Control Strategy for Hybrid Electric Vehicle Powertrain. 2015;3:362-70.
[39] Quan F, Rui H, Fenfang C, Long L, Xiaoli Y. Thermal management strategy of battery electric vehicle powertrain based on model predictive control %J Modern Machinery. 2019:8-15.
[40] Huo W, He H, Sun FJRA. Electrochemical–thermal modeling for a ternary lithium ion battery during discharging and driving cycle testing. 2015;5:57599-607.
[41] Tsokolis D, Tsiakmakis S, Dimaratos A, Fontaras G, Pistikopoulos P, Ciuffo B, et al. Fuel consumption and CO2 emissions of passenger cars over the New Worldwide Harmonized Test Protocol. 2016.